Progress In Electromagnetics Research C, Vol. 50, 103–111, 2014

A Millimeter-Wave Wideband High-Gain Antenna Based on the Fabry-Perot Resonator Antenna Concept

Yuehe Ge* **and Can Wang**

Abstract—A compact millimeter-wave (MMW) wideband high-gain antenna is proposed and implemented. The development is based on the design principle of wideband Fabry-Perot resonator antennas (FPRAs). The antenna consists of triple-layer dielectric slabs and a PEC ground, and it is fed by a rectangular waveguide. All slabs are used to form the superstrate that exhibits the increasing reflection phase at the designed frequency band. Size reduction of the superstrate is carried out to enhance the bandwidth of the antenna. The effect of ground size and resonant frequency shift due to size reduction of the superstrate were studied. A wide bandwidth of over 30% was finally obtained, and measurements of the fabricated prototype validate the theory and simulation results.

1. INTRODUCTION

Fabry-Perot (FP) cavity was first applied to enhance the gain of antennas in 1956 [1]. Afterwards, dielectric Fabry-Perot resonator antennas (FPRAs) were studied [2]. Recently, with the progress of the research on photonic band-gap (PBG) and electromagnetic band-gap (EBG) materials, artificial materials have been applied to the development of high-gain, wideband [3–10] and multiband FPRAs [11, 12]. Advantages of such antennas include structural simplicity, low cost and ease of fabrication as compared to the conventional planar antenna arrays.

Due to the inherent narrow bandwidth of Fabry-Perot cavity, most FPRAs in the literature are narrow band. To tackle this problem, an active reconfigurable FPRA is developed to achieve a bandwidth of 13.5% [3]. The dual-resonator configuration has been implemented [4] and analyzed in detail in [5] for wideband FPRAs. A patch array feeding is applied to a FPRA with a dual-resonator to obtain a bandwidth of 13.2% [4]. The EBG structures with increasing reflection phase have been developed [6–9] using multi-layer superstrates, leading to wideband Fabry-Perot cavities and hence wideband FPRAs. Recently, the design principle for EBG structures with increasing reflection phase was implemented [10], and a single dielectric layer with dual dipole arrays etched on its two sides was developed to form wideband FPRAs [10], due to its increasing reflection phase in the operating frequency band.

Recently, millimeter-wave (MMW) Fabry-Perot resonator antennas have also been investigated [13, 14]. Low-profile directive FPRAs [14], fed by a patch antenna array or a slot array, are developed for various millimeter-wave systems. In this paper, wideband millimeter-wave FPRAs are investigated and implemented. Due to the relatively high metallic loss in the millimeter-wave band, dielectric slabs without any metallic coating are applied to the implementation. Although multiple dielectric slabs will increase the profile of the FPRAs, a compact configuration can still be obtained at millimeter-wave band due to their small wavelengths. In the proposed FPRA, three dielectric slabs are applied to generate the increasing phase at the designated frequency band. Size reduction technique together with the increasing phase on the dielectric superstrate will be applied to tackle one of limitations of FPRAs, as mentioned in [10], the deteriorated radiation pattern at higher frequencies, due to the

Received 20 March 2014, Accepted 7 May 2014, Scheduled 16 May 2014
* Corresponding author: Yuehe Ge (yuehe@ieee.org).
The authors are with the College of Information Science and Engineering, Huaqiao University, Xiamen, Fujian 361021, China.

out-of-phase leaky waves on the surface of the superstrate, and this will further significantly enhance the effective 3-dB gain bandwidth of the proposed antenna. The combination of the two techniques results in a bandwidth of over 30% for a high-gain MMW antenna, which, to the best of the authors' knowledge, is the widest bandwidth of this kind of antennas.

2. ANTENNA DESIGN OF 1D MMW FPRA

2.1. Design Strategy

Conventional Fabry-Perot resonator antennas were theoretically analyzed in [1, 2], while wideband 1D FPRAs with dual-resonator were first implemented in [4], then analyzed and discussed in detail in [5]. The main disadvantage of 1D FPRAs is their high profile, because almost all of them are composed of multi-layer dielectric slabs. However, there exists another major disadvantage, which has been seldom mentioned in open literatures. The sidelobe levels increase dramatically at high frequencies. It is well known that the pencil beam with low-level sidelobes is required for directive antennas or high-gain antennas. In FPRAs, the bandwidth is normally defined by the 3-dB gain operating band. The input impedance bandwidth should cover the 3-dB gain bandwidth. However, it should be noted [10] that the 3-dB gain bandwidth may be no longer the best figure of merit to evaluate the FPRA, and a new term of "effective bandwidth" has been proposed in [10] to define the bandwidth of FPRAs. To illustrate this issue, the directivity and radiation patterns at four typical frequencies of an FPRA example are plotted in Fig. 1. It can be seen in Fig. 1(a) that the 3-dB gain or directivity bandwidth is within the rectangular frame. The resonant frequency of the Fabry-Perot cavity is f_r. Frequency f_{c1} is lower than f_r while two other frequencies f_{c2} and f_{c3} are higher than f_r. The radiation patterns at the four frequencies f_{c1}, f_r, f_{c2}, and f_{c3} are shown in Fig. 1(b). One can see that patterns at f_{c1} and f_r are typical pencil beams, but those at f_{c2} and f_{c3} have high-level sidelobes, especially the pattern at f_{c3} where the sidelobe level is similar to that of the main lobe.

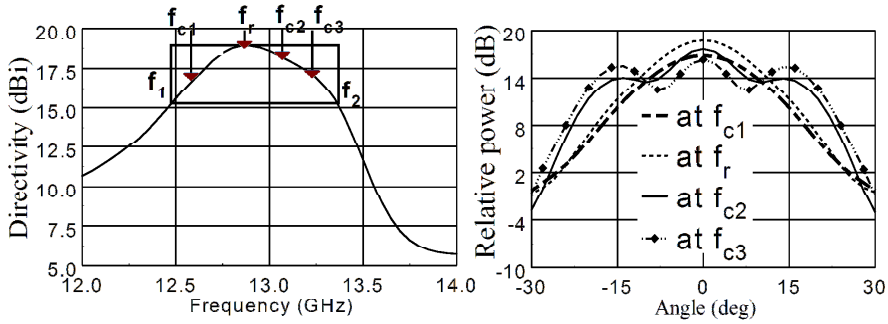

Figure 1. (a) Directivity v.s. frequency; (b) Radiation patterns.

The reason for FPRAs with high-level sidelobes at the upper band is that the waves on the surface of the EBG structure are out-of-phase. As we know, FPRAs are resonant antennas. When the operating frequency is lower than the resonant frequency of the Fabry-Perot cavity, the waves on the surface of the superstrate of the Fabry-Perot cavity are in-phase, and high gain and pencil-beam radiation patterns can be obtained. When the operating frequencies are gradually higher than the resonant frequency, the waves on the surface of the superstrate are out-of-phase, and the gain will gradually decrease, the level of sidelobes increase. As can be seen in Fig. 1(b), the level of sidelobes of radiation patterns will increase when the operating frequency is over the resonant frequency, though the gain is still within the 3-dB gain bandwidth.

To solve the problem and broaden the bandwidth of the FPRAs, superstrates with increasing phase were proposed [15] and implemented [6–10], where the Fabry-Perot cavity is able to or close to resonate at a wideband frequency band, resulting in wideband FPRAs. A promising design in [10] provides an effective bandwidth of 12.6% and a 3-dB gain bandwidth of 15.7%. To further enhance

the bandwidth, the compact-size EBG structure has been demonstrated [16] to theoretically provide a bandwidth of about 30%. However, to the best of the authors' knowledge, there is no experimental results to demonstrate the wideband performance of FPRAs with the compact-size EBG superstrate in open literature.

In this paper, wideband 1D millimeter-wave FPRAs are experimentally implemented based on the combination of the design principles presented in [10, 16]. The relation of the bandwidth and the size of the superstrate will be studied in detail. The design strategy is outlined below

1) The EBG structure (superstrate) is composed of dielectric slabs, to avoid the metallic loss.
2) Multi-layer dielectric slabs are applied to provide increasing phase and high gain at the designated frequency band.
3) Size reduction for the superstrate is applied to seek wide bandwidth with appropriate gain.

2.2. Design of the 1D Superstrate with Increasing Phase

A clear dual-resonant-element method to obtain increasing phase is proposed [10] for a single dielectric slab loaded with two arrays of dipoles on its two sides. For 1D superstrates [4, 5] where pure dielectric slabs are applied, the additional resonant cavity will lead to the increasing phase [5] around the resonant frequency. Nevertheless, the increasing phase can also be generated by multi-layer dielectric slabs without any resonant element on them and resonant cavities inside. The dual-resonant-element method [10] proposes that a single dielectric slab with two dipole arrays on its two sides will obtain the increasing reflection phase if the two dipole arrays resonate at two different but close frequencies. By extending the method to 1D superstrates, the increasing phase can be obtained on the surface of two different dielectric slabs, if they resonate at two different but close frequencies and are separated by an appropriate air gap.

It is well known that a planar dielectric slab with the thickness of $0.25\lambda_g$ will strongly resonate. Two such slabs can be applied to achieve the increasing phase if they resonate at different but close frequencies. An example is given to demonstrate the validity of this method. Figs. 2(a) and 2(b) show the models of the unit cell for one and two dielectric slabs respectively, which can be applied to calculate their reflection and transmission respectively. In the two models, PEC and PMC walls are applied to the four boundaries surrounding the unit cells, in order to obtain the reflection and transmission of slabs with infinite size [11]. Given that two slabs have the same permittivity of 10.5 and different thicknesses, 1.27 mm and 1.1 mm, respectively, the reflection magnitudes are simulated and plotted in Fig. 2(c). Two strong resonances at frequencies 36.3 GHz and 41.8 GHz, respectively, can be found. By placing the two slabs in parallel with $d = 2.5$ mm (about $\lambda/4$ at 30 GHz), the model in Fig. 2(b) is applied to obtain the reflection magnitude and phase, which are also plotted in Fig. 2(c). It can be seen that two increasing phases are achieved in the reflection phase curves obtained from Port 1 and 2 reflectively.

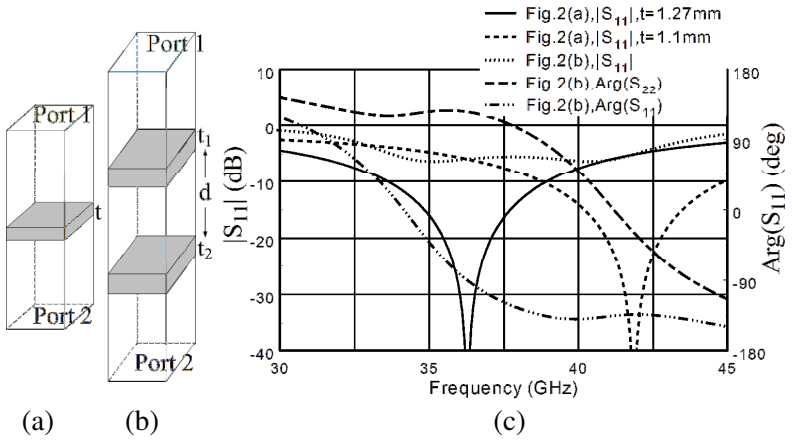

Figure 2. (a) A unit cell model for a single infinite-size slab; (b) A model for two parallel infinite-size slabs; (c) Reflection magnitudes and phases for the designated slabs.

2.3. Antenna Structure

The strategy described above was applied to design a compact wideband millimeter-wave Fabry-Perot resonator antenna that operates at the frequency band of 30–40 GHz. The proposed FPRA configuration is shown in Fig. 3, where three dielectric slabs form the superstrate. Two slabs are placed with no air gap between them, and the third slab is suspended above the second one with a height of h_2. The cavity between the PEC ground and Slab 1 has a height of h_1. The standard waveguide WR28 is used to feed the antenna. Metallic irises are loaded on the feeding aperture (open end) of the WR28 on the surface of the ground conductor to enhance the impedance matching.

Increasing reflection phase on the dielectric superstrate can be obtained using the method described in Section 2.2. However, the dielectric slabs with the designed parameters are sometimes not directly available in the markets. In the practical design, the method in Section 2.2 is slightly modified. The thickness and permittivity of one of the slabs are slightly changed so that the designed slabs are commercially available with an appropriate cost, without compromising the performance of the required increasing phase in the designated frequency band. In the final design, three dielectric slabs are applied to create the required reflection phase. The dielectric constants and thicknesses for the three slabs are determined to be 10.5, 2.94, and 10.5 and *0.6 mm*, *1 mm*, and *1.27 mm*, respectively. The simulated reflection magnitude and phase of the proposed 1D EBG superstrate, varying with parameter h_2, are plotted in Fig. 4.

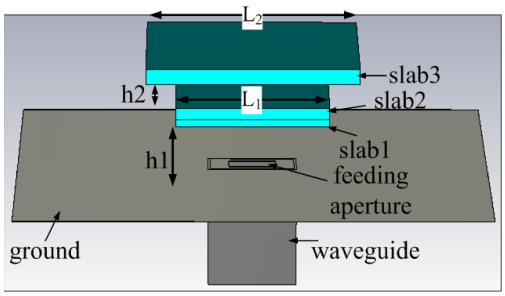

Figure 3. Configuration of the proposed MMW FPRA.

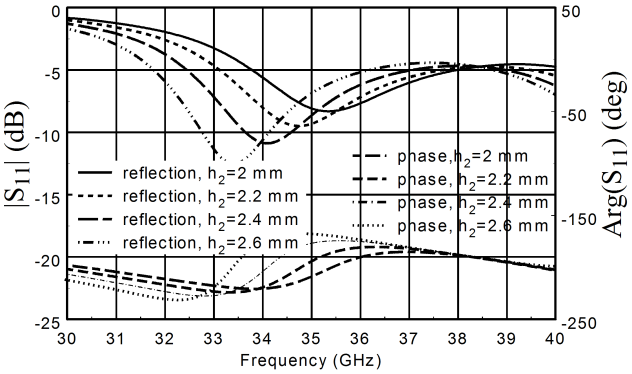

Figure 4. Reflection magnitudes and phases of the proposed 1D EBG structure.

2.4. Effects of the Size Reduction of the Superstrate

Size reduction of the superstrate can extremely enhance the bandwidth of the FPRAs, as theoretically demonstrated in [16]. Due to truncating the superstrate, the adverse effect of the out of phase on the radiation patterns at the upper frequency band can be weakened significantly, resulting in the enhancement of the effective 3-dB gain bandwidth. Here the effect of the size reduction of the superstrate on the bandwidth enhancement is quantitatively studied, based on simulations from Ansoft HFSS. During the study, the parameter h_1 varies between *4.3 mm* and *4.7 mm* and h_2 between *2.3 mm* and *2.7 mm*, to guarantee an optimum result between the peak gain and bandwidth for each size of the superstrate. The results are shown in Fig. 5. It can be seen that the bandwidth will be enhanced significantly while the peak gain decreases slowly with the size reduction of the superstrate. When the size is between $1.3\lambda \times 1.3\lambda$ and $1.8\lambda \times 1.8\lambda$, the peak gain will change a little while the bandwidth will increase significantly.

Further study was performed by slightly changing the size of the Slab 1, 2, and 3 separately to seek a better gain with a promising bandwidth and radiation patterns. It was found that increasing the size of Slab 3 to 1.8λ while keeping those of Slab 1 and 2 at 1.3λ will give a stable gain or directivity over the operating band. Fig. 6 shows the varied directivities for FPRAs with different superstrate sizes. It can be seen that the FPRA with $L_1 = 13\,\text{mm}$ (1.3λ at 30 GHz) and $L_2 = 18\,\text{mm}$ (1.8λ) exhibits

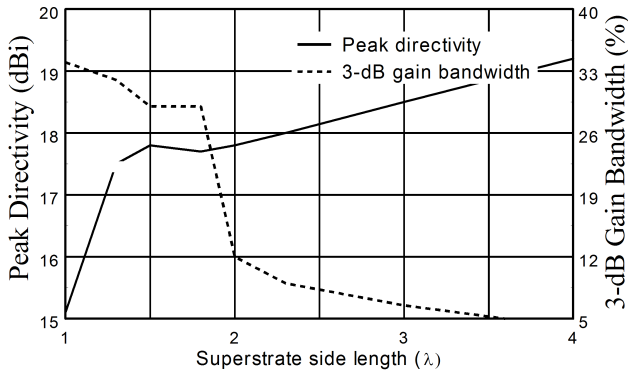

Figure 5. Peak directivity and bandwidth varies with the superstrate size.

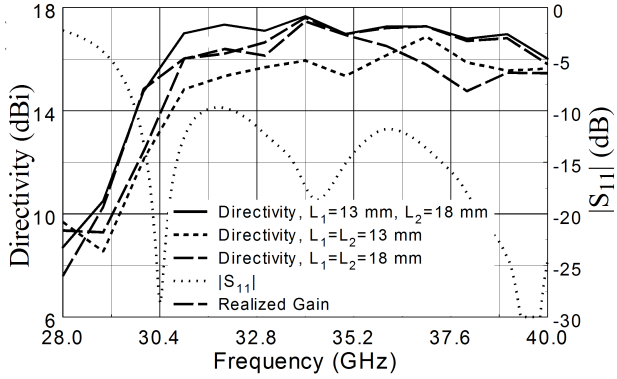

Figure 6. Directivities of FPRAs with different superstrate sizes.

a more stable directivity and a better peak directivity over the band of 30–40 GHz than FPRAs with $L_1 = L_2 = 18$ mm or $L_1 = L_2 = 13$ mm. In the simulation, the size of the ground plane is $3\lambda \times 3\lambda$. The simulated reflection coefficients of the FPRAs for the three different sizes are found similar, and hence only that for the superstrate with $L_1 = 13$ mm and $L_2 = 18$ mm is plotted in Fig. 6 for bandwidth comparison between those of the 3-dB directivity and the impedance matching. The simulated realized gain for the FPRA with $L_1 = 13$ mm and $L_2 = 18$ mm is also plotted in Fig. 6 for comparison.

The reflection phase of the superstrate obtained in Section 2.2 is based on the models shown in Figs. 2(a) and 2(b), which assume that the superstrate has an infinite size. Nevertheless, the size reduction of the superstrate might affect the results shown in Figs. 2(c) and 4, and hence the performance of the associated FPRAs. Therefore, the effect of the size reduction of the superstrate on its reflection phase should be studied. However, models in Figs. 2(a) and 2(b) cannot be applied to characterize the superstrate with a finite size. It is also difficult to directly obtain the reflection phase from a superstrate with a finite size.

It is well known now that the peak gain or directivity of a FPRA occurs at the resonant frequency of the Fabry-Perot cavity formed by the superstrate and the ground. The resonant frequency of a Fabry-Perot cavity can vary when the size of the superstrate changes. Therefore, the peak directivity of a FPRA will vary with the size of the superstrate, thus the change of the reflection phase can be derived from the variation of the peak directivity of a FPRA with a finite size superstrate. A FPRA example is presented here to demonstrate the variation of the resonant frequency of a Fabry-Perot cavity and hence the reflection phase of the superstrate, with the superstrate size. The FPRA has a similar configuration to that shown in Fig. 3, but the superstrate is composed of a single dielectric square slab in this case. The square slab has a dielectric constant of 10.2 and a thickness of 1 mm. The height of the cavity formed by the slab and PEC ground is 4.6 mm. The side length of the square superstrate and the ground varies between 1λ and 6λ. The simulated results are plotted in Fig. 7. As can be seen, the resonant frequency increases with the reduction of the superstrate size. One can derive from this that the frequency band of the increasing phase, shown in Figs. 2(c) and 4, will shift to the upper band with reducing the size of the superstrate.

2.5. Effect of the Size of the Ground

It is demonstrated in Section 2.4 that the bandwidth of the FPRAs can be significantly enhanced by reducing the size of the superstrate. In the study of the bandwidth enhancement, the size of the superstrate is gradually reduced while that of the ground is always $6\lambda \times 6\lambda$. The effect of the ground size on the performance of the proposed FPRA will be studied in this section.

In the study, the parameters of the proposed FPRA, shown in Fig. 3, are chosen based on the study in Section 2.4. They are $L_1 = 13$ mm, $L_2 = 18$ mm, $h_1 = 4.6$ mm and $h_2 = 2.6$ mm. The permittivity and thickness of the three slabs are kept the same as those in Section 2.3. The ground size will gradually vary from $6\lambda \times 6\lambda$ to $1.8\lambda \times 1.8\lambda$, to strike a balance between the antenna performance and the size.

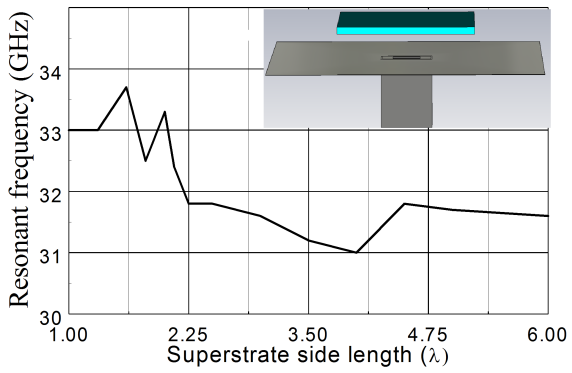

Figure 7. Resonant frequency v.s. the superstrate size of a FPRA.

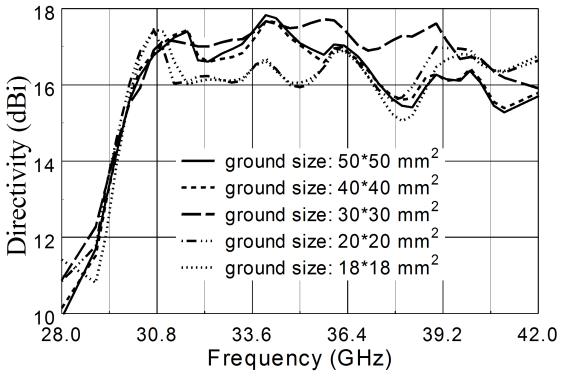

Figure 8. Effect of the ground size on the directivity of the proposed FPRA.

The curves of the directivity of the proposed FPRA versus frequency for different ground sizes, obtained from the simulations of Ansoft HFSS, are plotted in Fig. 8. It can be seen that the FPRA with a ground of $30 \times 30\,\mathrm{mm}^2$ ($3\lambda \times 3\lambda$ at 30 GHz) gives a stable directivity over the frequency band of 30–40 GHz, showing the best result among the FPRAs with different ground sizes. The radiation patterns are formed by both the wave above the superstrate and that outside the Fabry-Perot cavity. The large ground size might cause out-of-phase between some waves outside the cavity and the wave above the superstrate at the higher band, while the small ground might result in that some waves outside the cavity cannot contribute to the formation of the gain in the broadside of the antenna.

3. EXPERIMENTAL RESULTS AND DISCUSSION

A prototype of the MMW FPRA design above was fabricated for measurements. The materials selected for the three dielectric slabs are *ARLON AD1000L02511* for Slab 1, *ARLON CLTE-XT04011* for Slab 2 and *ARLON AD1000L05055* for Slab 3, whose dielectric constants are 10.5, 2.94, and 10.5, respectively. The thicknesses for them are *0.635 mm*, *1.04 mm*, and *1.27 mm*, respectively. Their surface sizes are $13 \times 13\,mm^2$ for Slab 1 and 2, and $18 \times 18\,mm^2$ for Slab 3. The size of the ground plane is $30 \times 30\,mm^2$. The parameters h_1 and h_2 are set to be *4.6 mm* and *2.6 mm*, respectively. A standard WR28 open-end rectangular waveguide is applied to feed the FPRA, which has an inner aperture size of $7.112 \times 3.556\,mm^2$. Copper tapes are placed on the feeding aperture to match the input impedance

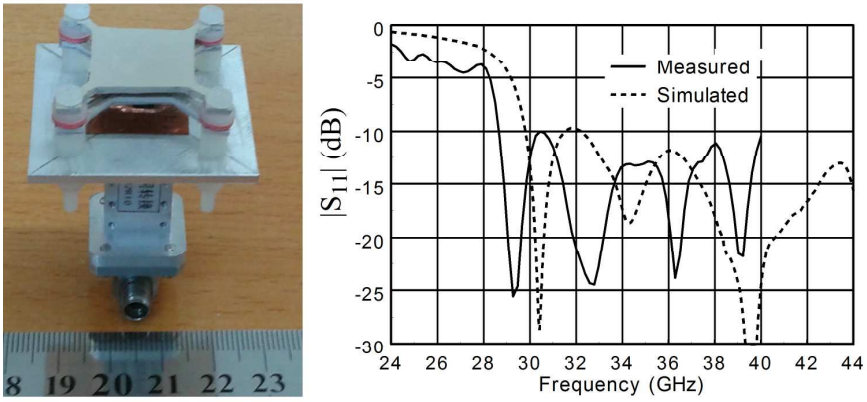

(a) (b)

Figure 9. (a) MMW FPRA prototype; (b) Measured reflection coefficient.

so that the feeding aperture size on the ground surface is $4 \times 2\,mm^2$. The picture of the prototype is shown in Fig. 9(a). As can be seen, all three square slabs extend from the four corners. Holes are drilled at the ends of all corner extensions for mounting. Plastic screws and spacers are used to fasten the slabs on the ground conductor and control the heights h_1 and h_2, respectively. The total volume of the FPRA above the ground plane is $18 \times 18 \times 10.145\,mm^3$ or $1.8\lambda_0 \times 1.8\lambda_0 \times 1.15\lambda_0$ at the lowest operating frequency of *30 GHz*.

The prototype was measured using Vector Network Analyzer Agilent E8363C, and the S_{11} result is plotted in Fig. 9(b). Due to the limited frequency range of the analyzer, the results above 40 GHz cannot be obtained. The measured bandwidth, determined by $S_{11} < -10\,dB$, is from *28.6 GHz* to *40 GHz*, up to 33.2%. For comparison, the theoretical result, obtained from commercial software Ansoft HFSS, is also plotted in Fig. 9(b), which shows a better impedance bandwidth. The difference between the simulation and the measurement might be caused by the tolerance of the fabricated superstrate and the feeding aperture, as well as the installation screws and spacers.

The radiation patterns were measured in an Anechoic Microwave Chamber. A far-field range was built to measure the radiation patterns. Vector Network Analyzer Agilent E8363C and gain horns SAS-588 (26.5 GHz–40 GHz) are employed in the range. Fig. 10 shows the measured radiation patterns of the FPRA prototype in the E- and H-planes at frequencies of *30 GHz*, *33 GHz*, *36 GHz* and *38 GHz*. It can be seen that reasonable radiation patterns are obtained. In the right side of each radiation patterns, there are relatively higher sidelobes, which are not obtained theoretically. The reason is that the spacers' lengths for installation of the three slabs are not exactly same so that they are not symmetrically mounted above the feeding aperture on the ground conductor. The gain of the FPRA was also measured over the band of *28–40 GHz* and the results are plotted in Fig. 11, together with the computed directivity, obtained from Ansoft HFSS, for comparison. The measurement shows a 3-dB

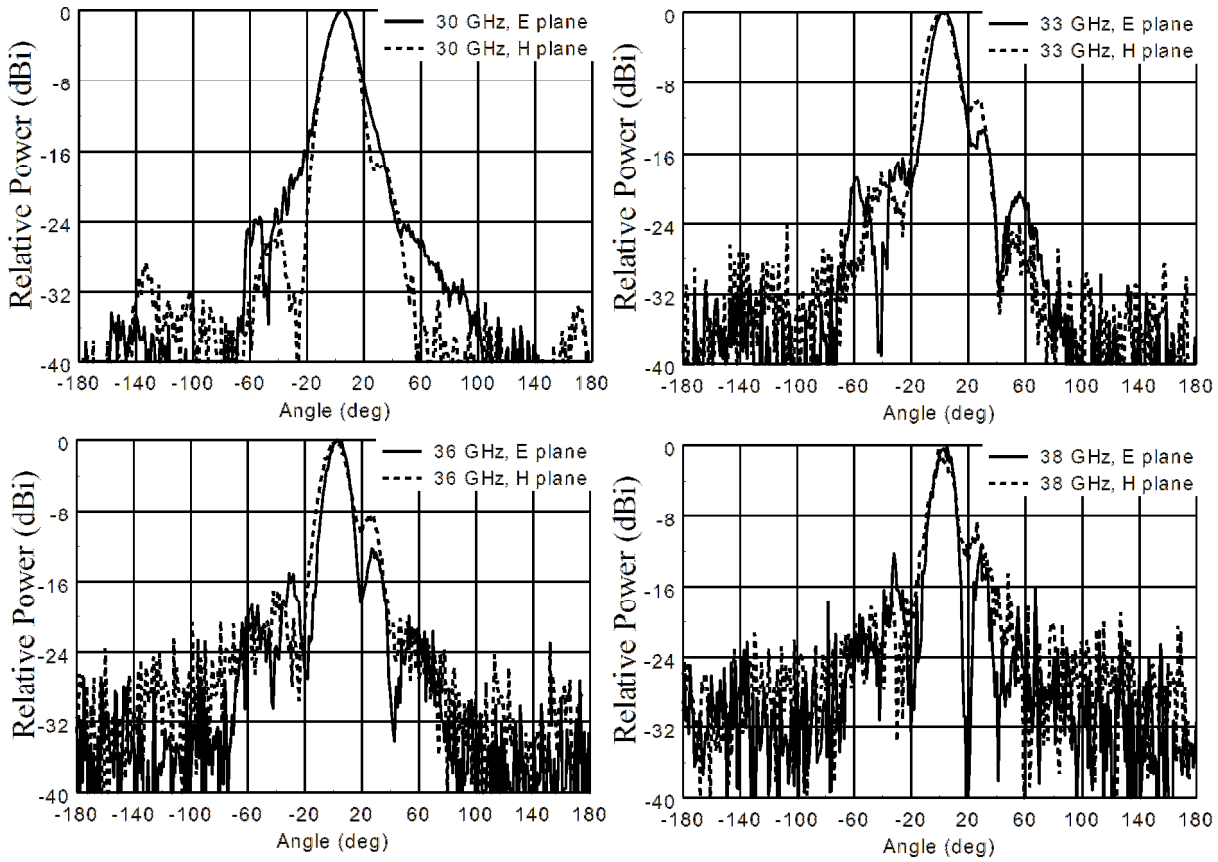

Figure 10. Measured radiation patterns at *30 GHz*, *33 GHz*, *36 GHz* and *38 GHz*.

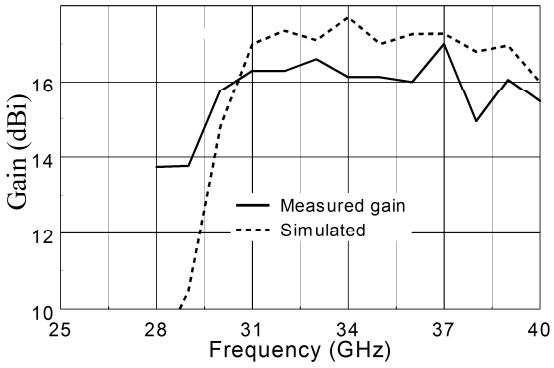

Figure 11. Measured gain and simulated directivity of the FPRA prototype.

gain bandwidth of about 32%, from 28.8 GHz to 40 GHz. Note that the gain above 40 GHz is still within the 3-dB gain bandwidth theoretically but not counted here due to the limitation of the test range.

In summary, the antenna design procedures are outlined here: 1) the design of the superstrate with increasing phase in the designated band; 2) the application of the size reduction of the superstrate to find the optimum results for the bandwidth and the gain or directivity, as demonstrated in Section 2.4; 3) the determination of the feeding mechanism.

The first procedure includes the material selection and determination of the distance between dielectric slabs. The superstrate with decreasing phase is also investigated using the method of size reduction of the superstrate, as demonstrated in [16]. It was found that based on our investigation, the 3-dB directivity bandwidth is not as wide as that using the superstrate with increasing phase. Another existing problem is that the radiation patterns at the higher band, as indicated in Section 2.1, will deteriorate. The selection of the feeding methods is found to be limited. Only FPRAs fed by the open rectangular waveguide are able to provide both wide bandwidth and good radiation patterns. Other feeding methods, such as stacked patch antennas [3], monopole antennas [10], etc., either cannot give good impedance matching over the 3-dB directivity bandwidth, or result in unexpected radiation patterns at the high band.

4. CONCLUSIONS

A millimeter-wave 1D wideband high-gain antenna is successfully developed using the FPRA concept. The design strategies are based on the increasing reflection phase in the designated frequency band and the size reduction of the superstrate of the FPRA. The increasing phase at the designated band is obtained using triple-layer dielectric slabs, without any resonant element on them and resonant cavities inside. Simulations demonstrate that extremely wide bandwidth can be obtained when the size of the FPRA's superstrate is about $1.3\lambda \times 1.3\lambda$, without compromising much the performance of the directivity and radiation patterns. Studies also show that the frequency band of the increasing phase will shift to higher with the size reduction of the superstrate. When the size of the square superstrate is between $1.3\lambda \times 1.3\lambda$ and $1.8\lambda \times 1.8\lambda$, there is a trade-off in obtaining the wide bandwidth and the high gain. When the sizes of the upper and lower slabs are $1.8\lambda \times 1.8\lambda$ and $1.3\lambda \times 1.3\lambda$ respectively and the ground size is $3\lambda \times 3\lambda$, the antenna exhibits a stable and higher gain over the entire bandwidth. Measurements of the prototype shows an operating impedance band of 28.6–40 GHz and a 3-dB gain band of 28.8–40 GHz, up to 32% bandwidth obtained, with a peak gain of 17 dBi.

ACKNOWLEDGMENT

This research was supported by the start-up grants (11BS301) of Huaqiao University, Xiamen 361021, China, Natural Science Foundation of Fujian Province (2012J01276), China, and Quanzhou Science and Technology Project (Z1424008) from Quanzhou 362021, China.

REFERENCES

1. Trentini, G. V., "Partially reflecting sheet array," *IRE Trans. on Antennas Propagat.*, Vol. 4, No. 10, 666–671, Oct. 1956.
2. Jackson, D. R. and N. Alexopoulos, "Gain enhancement methods for printed circuits antennas," *IEEE Trans. on Antennas Propagat.*, Vol. 33, No. 9, 976–987, Sep. 1985.
3. Weily, A. T., S. Bird, and Y. J. Guo, "A reconfigurable high-gain partially reflecting surface antenna," *IEEE Trans. on Antennas Propagat.*, Vol. 56, No. 11, 3382–3390, Nov. 2008.
4. Weily, A., K. P. Esselle, B. C. Sanders, and T. S. Bird, "High-gain 1D EBG resonator antenna," *Microw. Opt. Technol. Lett.*, Vol. 47, No. 2, 107–114, Oct. 2005.
5. Al-Tarifi, M. A., D. E. Anagnostou, A. K. Amert, and K. W. Whites, "Bandwidth enhancement of the resonant cavity antenna by using two dielectric superstrates," *IEEE Trans. on Antennas Propagat.*, Vol. 61, No. 4, 1898–1908, Apr. 2013.
6. Feresidis, P. and J. C. Vardaxoglou, "A broadband high-gain resonant cavity antenna with single feed," *Proc. EuCAP 2006*, 1–5, Nice, France, 2006.
7. Boutayeb, H., T. A. Denidni, and M. Nedil, "Bandwidth widening techniques for directive antennas based on partially reflecting surfaces," *Progress In Electromagnetics Research*, Vol. 74, 407–419, 2007.
8. Moustafa, L. and B. Jecko, "EBG structure with wide defect band for broadband cavity antenna applications," *IEEE Antennas Wireless Propagat. Lett.*, Vol. 7, 693–696, 2008.
9. Wang, N.-Z., C. Zhang, Q.-S. Zeng, N.-Q. Wang, and X.-J. Dong, "New dielectric 1D EBG structure for the design of wideband resonator antennas," *Progress In Electromagnetics Research*, Vol. 141, 233–248, 2013.
10. Ge, Y., K. P. Esselle, and T. S. Bird, "The use of simple thin partially reflective surfaces with positive reflection phase gradients to design wideband, low-profile EBG resonator antennas," *IEEE Trans. on Antennas Propagat.*, Vol. 60, No. 2, 743–750, Feb. 2012.
11. Ge, Y., K. P. Esselle, and T. S. Bird, "A method to design dual-band, high-directivity EBG resonator antennas using single-resonant, single-layer partially reflective surface," *Progress In Electromagnetics Research C*, Vol. 13, 245–257, 2010.
12. Zeb, A., Y. Ge, K. P. Esselle, Z. Sun, and M. E. Tobar, "A simple dual-band electromagnetic band gap resonator antenna based on inverted reflection phase gradient," *IEEE Trans. on Antennas Propagat.*, Vol. 60, No. 10, 4522–4529, Oct. 2012.
13. Lee Y., X. Lu, Y. Hao, S. Yang, J. R. G. Evans, and C. G. Parini, "Low-profile directive millimeter-wave antennas using free-formed three-dimensional (3-D) electromagnetic bandgap structures," *IEEE Trans. on Antennas Propagat.*, Vol. 57, No. 10, 2893–2903, Oct. 2009.
14. Hosseini, S. A., F. Capolino, and F. D. Flaviis, "A 44 GHz single-feed Fabry-Pérot cavity antenna designed and fabricated on quartz," *IEEE Antennas and Propagation Society (AP-S) International Symposium*, 1285–1288, Spokane, Washington, USA, Jul. 3–8, 2011.
15. Feresidis, A. P. and J. C. Vardaxoglou, "High gain planar antenna using optimised partially reflective surfaces," *IEE Microw. Antennas Propagat.*, Vol. 148, No. 6, 345–350, 2001.
16. Lee, Y. J., J. Yeo, R. Mittra, and W. S. Park, "Application of electromagnetic bandgap (EBG) superstrates with controllable defects for a class of patch antennas as spatial angular filters," *IEEE Trans. on Antennas Propagat.*, Vol. 53, No. 1, 224–235, Jan. 2005.